IEEE Access
Multidisciplinary | Rapid Review | Open Access Journal

Received 7 August 2023, accepted 22 August 2023, date of publication 6 September 2023, date of current version 14 September 2023.

Digital Object Identifier 10.1109/ACCESS.2023.3312619

RESEARCH ARTICLE

An RNS-Based Initial Absolute Position Estimator for Electrical Encoders

GIAN CARLO CARDARILLI[1], (Member, IEEE), LUCA DI NUNZIO[1], ROCCO FAZZOLARI[1], DANIELE GIARDINO[1], MARCO RE[1], (Member, IEEE), ALBERTO NANNARELLI[2], (Senior Member, IEEE), AND SERGIO SPANÒ[1]

[1]Department of Electronic Engineering, University of Rome "Tor Vergata," 00133 Rome, Italy
[2]Department of Applied Mathematics and Computer Science, Danmarks Tekniske Universitet, 2800 Lyngby, Denmark

Corresponding author: Luca Di Nunzio (di.nunzio@ing.uniroma2.it)

ABSTRACT In digital systems, the Residue Number System (RNS) represents an interesting alternative to the traditional two's complement representation. Its performance and low-power properties have attracted significant research interest over the years. In this paper, RNS is used to estimate the angular position of a multi-trace electrical encoder (EE), an electro-mechanical device to measure angles at high precision widely used, for example, in antennas on-board satellites. The model of this system presents cyclic characteristics and, consequently, allows efficient use of modular arithmetic for its description. The RNS is applied to EEs equipped with more than two plates, and the absolute angle reconstruction is performed by using the Chinese Remainder Theorem (CRT). Furthermore, the use of RNS allows detection and mitigation solutions for errors due to encoders' non-idealities and electrical noise. In this noisy context, we provide a detailed analysis of the performance of the system and propose a more robust, flexible, and easy-to-implement solution compared with the traditional methods. The results show that the RNS-based system can attenuate the noise, measure accurately the angles, and improve the overall performance.

INDEX TERMS Angle measurement, Chinese reminder theorem (CRT), electrical encoder, error detection, modular arithmetic, residue number system (RNS).

I. INTRODUCTION

In the last decades, the Residue Number System (RNS) has been extensively used in digital systems as an alternative to the traditional Two's Complement System (TCS) representation [1], [2], [3].

For operations on integers of large dynamic range (a large number of bits), the advantage of the RNS is that operations such as addition and multiplication are computed in parallel in each path, or channel, corresponding to the components of the RNS base [1]. Since the dynamic range of the single components of the RNS base is significantly smaller than the dynamic range of the whole system, in the parallel channels, the carry chains are shorter and the arrays smaller reducing the delay and the power dissipation in the computation data path.

The associate editor coordinating the review of this manuscript and approving it for publication was Ganesh Naik.

These advantages made the RNS an interesting solution for increasing the speed and optimizing the power consumption of several applications including Digital Signal Processing (DSP) systems, as in the case of digital filters, and other architectures [4], [5], [6], [7]. High-speed and low-power DSP systems are today the main field of application for RNS and are well studied in the literature [8], [9], [10].

However, promising fields of application for RNS are systems with behavior that follows a periodic (modular) law. In these cases, the development of an RNS-based model helps the designer to master the true nature of the problem, obtaining more efficient and more adaptable algorithms [11].

In this context, in [12] the authors took advantage of the RNS representation for developing an algorithm for efficiently estimating the initial absolute position of a two-trace Electrical Encoder (EE), an electro-mechanical device used for precise measurement of angles.

Thanks to their reduced cost, electrical encoders are widely used, and often preferred, to other encoder typologies, for example, optical ones. The application fields are all those requiring the measurement of an angle, such as the measuring of the onboard antenna's pointing system in satellites.

The electrical encoders are low-cost devices, but they are less precise than their optical counterparts. For this reason, several techniques have been developed to increase precision by keeping costs down. Among these techniques, there is the use of a *multi-trace* (more than two) approach, in which the absolute angle is reconstructed by combining more measurements on different *tracks*, and the high derivative approach, where the sensitivity is increased by increasing the derivative of the signal with respect to the angle. This latter approach is implemented by increasing the number of revolutions of the sinusoidal shape of the tracks.

Indeed, the performance of these encoders can be enhanced by a) increasing the number of measurement positions for the single track, whose average gives the angular value, b) varying the number of tracks, and c) increasing the number of sinusoidal revolutions on the track. All the previous methods improve the performance of the encoder but they also increase the electronic and mechanical requirements and, ultimately, the cost. Therefore, for each application class, an appropriate combination of the number of tracks and number of revolutions must be found. Unfortunately, the methods currently used in commercial encoders are not easily generalizable regarding the number of traces and number of revolutions. This makes it challenging to adapt these methods to devices with different parameters. For this reason, in this paper, the authors propose an RNS-based method that offers inherent flexibility and scalability in absolute angle reconstruction. Unlike conventional methods that rely on complex analyses of cases and sub-cases, RNS provides a theoretical structure that generalizes to all possible scenarios. By applying the RNS to the problem analysis, the authors were able to leverage its characteristics and develop an algorithm adaptable to different numbers of tracks and different numbers of revolutions for each individual track. Consequently, this algorithm can be scaled to be applied to any number of traces, making it flexible for encoders with different performance levels. Each track requires an RNS modulus, so if there are three traces, three RNS moduli are used. Adapting to different numbers of revolutions is achieved simply by changing the values of the RNS moduli used. In contrast, traditional methods lack flexibility and scalability, as their memory content is tailored to a specific number of tracks and revolutions. Moreover, using the modeling proposed in the paper, it is possible to apply all the methods developed for error detection and correction methods present in the literature for RNS systems.

The paper is organized as follows: in Section II and Section III, we introduce the EE and give background information on the RNS. In Section IV, we present and describe the proposed algorithm, and in Section V we perform a detailed analysis of its performances in presence of noise, together with a proposed hardware solution for error detection and mitigation. In Section VI, we discuss the optimal choice of the RNS moduli for the EE, and, in Section VII, we draw the conclusions.

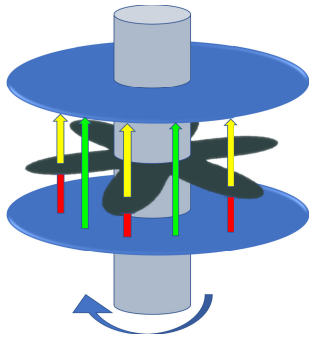

FIGURE 1. Basic scheme of a rotary electrical encoder [14].

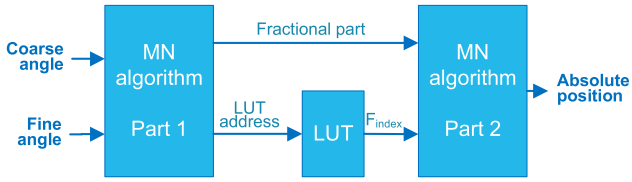

FIGURE 2. Basic scheme of the MN algorithm.

II. ELECTRICAL ENCODER: DESCRIPTION AND OPERATIONS

The rotary Electrical Encoder is implemented by 3 or 2 plates connected to a rotating central shaft, as sketched in Figure 1. Both plates include a space/time-modulated electric field inside a shielded enclosure. The total electric field is integrated and converted into a current proportional to the sine and cosine of the actual angle, corresponding to the position of the plates.

The EE is built at least with two different plates: a coarse mode plate and a fine mode plate. The rotation of the plates generates geometrical sinusoidal profiles and corresponding electrical fields. At the system start, the coarse mode is used to generate the first coarse angle value. Afterward, the combination of the coarse value with the angle obtained in fine mode gives the starting absolute position with high accuracy and resolution.

For estimating the absolute position, commercial devices adopt a technique based on the MN algorithm [15], [16] which uses the information coming from the coarse and fine channels to detect the correct angle by the M and N (with M<N) sine and cosine revolution periods.

To provide unambiguous readings over 360 degrees, M and N must be co-prime, i.e., no common factors. The parameter M typically ranges from 1 to 7, and N from 16 to 128.

The block diagram of the MN algorithm, sketched in Figure 2, requires a number of scaling and add/subtract operations on *coarse* and *fine* measured angles plus a large Look-Up Table (LUT) to find the F_{index} parameter to determine the absolute position. The large LUT is stored in

memory, and its values need to be recomputed if M or N, or both, are changed. In other words, a large part of the algorithms depends on the values stored in the table, making the system not easily reconfigurable.

The main steps of the MN algorithm for a two plates encoder based on M = 32 (number of revolution periods of fine angle) and N = 3 (number of revolution periods of coarse angle) are depicted below:

1) After measuring the local angle on each plate (coarse angle on 3-revolution plate and fine angle on 32-revolution plates), is calculated the parameter $Diff = \frac{coarse\_angle}{M} - \frac{fine\_angle}{N}$
2) Depending on the value of parameter Diff and according to the values stored in a LUT table, the parameter fine index is generated.
3) In the last step the absolute angle is calculated by using the following equation: $AbsoluteAngle = \left(F_{index} + \frac{F_{EA}}{360}\right) \cdot \frac{360}{F_{EC}}$ where $F_{EC} = N = 32$ and F_{EA} is the angle measured on the fine angle, i.e. on the 32-revolution plate. In this case, the algorithm needs both a 34-locations table to store the fine index values and an addressing logic to read them.

It can be seen from the procedure described above that the use of an EE having more than two plates requires adapting the entire algorithm, re-designing the control logic, and using a bigger LUT. In the following, we will show how the use of an RNS-based algorithm can lift the limitations of the MN algorithm. Namely, the RNS can be applied to a system with three or more plates, and the large LUT is eliminated. Furthermore, the RNS is used to increase the robustness of the measurements.

III. RNS BACKGROUND

RNS is a non-positional and non-weighted number system defined by a p-tuple of relatively prime integers $\{m_1, m_2, \ldots, m_p\}$ called moduli and constituting the RNS base [1], [17]. The product of all moduli in the RNS base defines the dynamic range M of the system:

$$M = \prod_{i=1}^{P} m_i \tag{1}$$

An arbitrary integer $X \in \{0, 1, \ldots, M-1\}$ has an unique representation given by the set of P *residues* r_i

$$X \xrightarrow[Encoding]{RNS} (r_1, r_2, \ldots, r_P) = \left(\langle X\rangle_{m_1}, \langle X\rangle_{m_2}, \ldots, \langle X\rangle_{m_P}\right) \tag{2}$$

where $\langle X\rangle_{m_i}$ is the operation X *modulus* m_i.

Unlike classical number systems (decimal, binary, etc.), RNS does not have a fixed radix and its main advantage is the decomposition of operations with a large dynamic range in modular operations in a reduced dynamic range that can be executed in parallel on the channels (paths) of the RNS base characterized by a reduced word-length

$$Z = X\ op\ Y \xrightarrow{RNS} \begin{cases} Z_{m_1} = \langle X_{m_1}\ op\ Y_{m_1}\rangle_{m_1} \\ Z_{m_2} = \langle X_{m_2}\ op\ Y_{m_2}\rangle_{m_2} \\ \ldots \quad \ldots \quad \ldots \\ Z_{m_P} = \langle X_{m_P}\ op\ Y_{m_P}\rangle_{m_P} \end{cases} \tag{3}$$

The main advantage of this decomposition is the computation of operations, such as addition and multiplication, in parallel in the modular channels described by (3), resulting in reduced delay and power consumption [3].

The reconstruction of Z starting from the residues z_i, can be performed using different techniques. Among these, one of the most common is the Chinese Reminder Theorem (CRT)

$$Z = \left\langle \sum_{i=1}^{P} z_i \cdot A_i \cdot \frac{M}{m_i} \right\rangle_M \tag{4}$$

where A_i are the *multiplicative inverses* defined as the smaller integer values such that $\langle A_i \cdot \frac{M}{m_i}\rangle_{m_i} = 1$ [1].

We put together (2), (3), and (4) in an example of RNS multiplication illustrated in Table 1.

TABLE 1. Example of RNS multiplication on the base {2, 3, 11}.

TCS multiplication
$X \times Y = 4 \times 13 = \mathbf{52}$

RNS encoding
RNS base: $m_i \in \{2, 3, 11\}, \quad M = 66$
$X = 4 \xrightarrow{RNS} x_i = \{0, 1, 4\}$
$Y = 13 \xrightarrow{RNS} y_i = \{1, 1, 2\}$

RNS multiplication
$z_1 = \langle x_1 \times y_1\rangle_{m_1} = \langle 0 \times 1\rangle_2 = 0$
$z_2 = \langle x_2 \times y_2\rangle_{m_2} = \langle 1 \times 1\rangle_4 = 1$
$z_3 = \langle x_3 \times y_3\rangle_{m_3} = \langle 4 \times 2\rangle_{11} = 8$

CRT (result)
Multiplicative inverses: $A_1 = 1, A_2 = 1, A_3 = 2$
CRT: $\langle (z_1 \cdot A_1 \cdot \frac{M}{m_1}) + (z_2 \cdot A_2 \cdot \frac{M}{m_2}) + (z_3 \cdot A_3 \cdot \frac{M}{m_3})\rangle_M =$
$= \langle (0 \cdot 1 \cdot 66/2) + \langle (1 \cdot 1 \cdot 66/3) + \langle (8 \cdot 2 \cdot 66/11)\rangle_{66} =$
$= \langle 0 + 22 + 96\rangle_{66} = \mathbf{52}$

IV. ABSOLUTE POSITION MEASUREMENT IN RNS

In [12], the authors took advantage of the RNS representation of the two angles for the development of a CRT-based reconstruction algorithm to measure the initial absolute position of an Electrical Encoder.

The EE model used in [12] may consist of two or more plates (see Figure 1) on which are engraved two traces (each one represented by a pair of sine and cosine waveforms) having respectively 3 (*coarse* measurement) and 32 (*fine* measurement) "revolutions per trace", or *rpt*, with respect to the absolute angle. The numbers of *rpt* of all traces are usually relative prime values, and this aspect allows us to easily apply an RNS representation.

In these EE, the *initial position* is computed by using all available traces, while the successive positions are computed

only by considering the trace with the higher number of *rpt* (i.e., 32 *rpt* for the EE cited in [12]).

The original algorithm for angle reconstruction proposed by the EE manufacturer uses a tabular approach that turns out to be less flexible with varying of EE models.

In the following, we describe the generalization of the algorithm to reconstruct the angle from its measurements for EE with an arbitrary number of tracks P, and how to mitigate the noise introduced by the measurements.

The proposed algorithm is more flexible and more reliable since it avoids the use of large portions of memory necessary for the tabular approach. In contrast, the RNS approach needs only a few parameters to be stored in the memory. Memory usage is very important, especially in space applications, where storage is a critical aspect.

A. GENERALIZATION OF ABSOLUTE POSITION MEASUREMENT

We assume an encoder with P traces, where each trace has a given number K_i of repeated patterns (rpt). The value of each K_i is not a random choice and it must be properly selected to allow the reconstruction of the actual value of the angle. This selection can be performed using a set of co-prime moduli m_i with $i = 1, \ldots, P$ following the Residue Number System (RNS) approach. With a modulus set like this, the number K_i of rpt for the i-th trace can be expressed as:

$$K_i = \frac{M}{m_i} \quad i \in 1, \ldots, P \tag{5}$$

where M and m_i are defined in (1), and P is the number of traces.

If $P = 2$, the number of periods of the first trace coincides with the modulus of the second trace and vice versa ($K_1 = m_2$ and $K_2 = m_1$). As a consequence, if $P = 2$, the number of rpt of traces must be relatively prime (for example, 3 and 32) since the Chinese Remainder Theorem (CRT) can be applied with relatively prime moduli.

For three or more traces, the numbers of rpt are not relatively prime since they are obtained by the product of relatively prime numbers (i.e., moduli). For example, for $P = 3$, if the moduli are $m_1 = 2$, $m_2 = 3$, $m_3 = 11$, the resulting rpt of the three traces are $K_1 = m_2 \cdot m_3 = 33$, $K_2 = m_1 \cdot m_3 = 22$, $K_3 = m_1 \cdot m_2 = 6$. The traces of this example are shown in Figure 3.

The use of this set of moduli corresponds to quantizing the complete angle (360°, or 2π) in M discrete values $0, Q, 2Q, \ldots, (M-1)Q$, as shown in Figure 4. As a consequence, the 360° angle is divided into M intervals. The corresponding quantization step $Q \in \mathcal{R}$ is given by the following expressions:

$$Q = \frac{360^\circ}{M} \quad \text{or} \quad Q = \frac{2\pi}{M}. \tag{6}$$

The angle Φ can be represented as a function of the quantization step Q. It is composed of the sum of an integer part (a multiple of Q) $\Phi_Q = k_\Phi \cdot Q$, and a fractional part

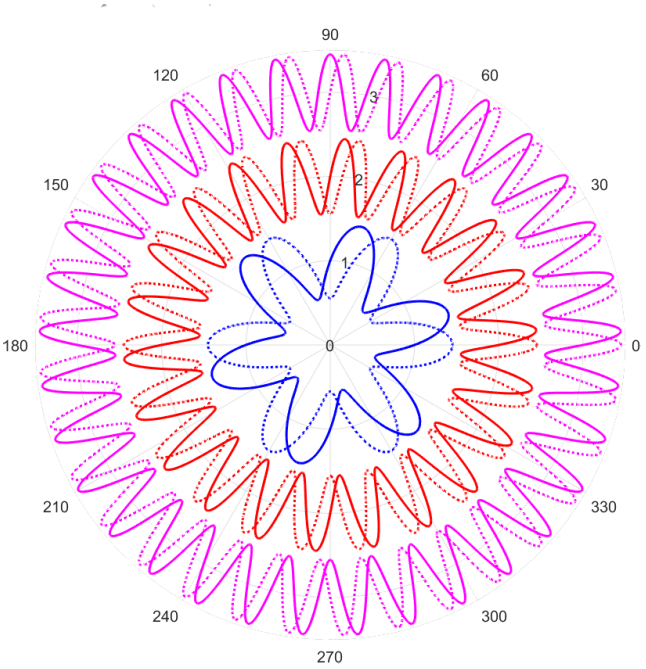

FIGURE 3. Example of EE with three sin/cos traces: $K_1 = 33$ *rpt* (purple lines) is the modulus 2, $K_2 = 22$ *rpt* (red lines) is the modulus 3 and $K_3 = 6$ *rpt* (blue lines) is the modulus 11.

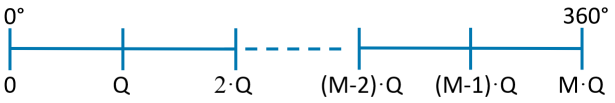

FIGURE 4. Shaft angle division in M intervals.

$$\Phi_\delta = \delta_\Phi \cdot Q < Q$$

$$\Phi = (\Phi_Q + \Phi_\delta) = (k_\Phi + \delta_\Phi) \cdot Q \tag{7}$$

with k_Φ an integer in the range $0 \leq k_\Phi < M$ and δ_Φ a fractional number in the range $0 \leq \delta_\Phi < 1$.

For each track, the EE provides the amplitudes $\cos(\varphi_i)$ and $\sin(\varphi_i)$ which are used for the extraction of the angle φ_i ($0 \leq \varphi_i < 360^\circ$)

$$\varphi_i = \frac{M}{m_i}[\Phi \mod_R (m_i \cdot Q)] \tag{8}$$

where $x \mod_R(y)$ represents the modulo operation between two real numbers, defined as

$$x \mod_R(y) := x - y \cdot \left\lfloor \frac{x}{y} \right\rfloor.$$

The reconstruction of Φ_Q in (7) from the read φ_i consists of the following three steps.

1) The actual angle γ_i is obtained by normalizing its value in the 360° range:

$$\gamma_i = \Phi \mod_R (m_i \cdot Q) = \frac{\varphi_i \cdot m_i}{M} \tag{9}$$

with $0 \leq \varphi_i < 360^\circ$. We refer to (9) as "normalization" in the following.

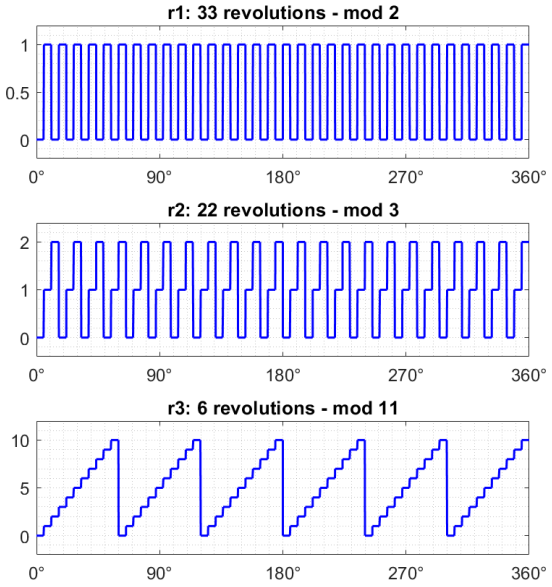

FIGURE 5. Residues' values for the 360° rotation of the EE shaft angle for the moduli set $m_i \in \{2, 3, 11\}$.

2) The RNS residues r_i are computed as the integer part of the normalized angles γ_i:

$$r_i = \left\lfloor \frac{\gamma_i}{Q} \right\rfloor = \left\lfloor \frac{\varphi_i \cdot m_i}{QM} \right\rfloor = k_\Phi \mod m_i \tag{10}$$

The Figure 5 depicts the values of the residues r_i when the rotor moves along the 360° absolute angle, for the moduli $m_i \in \{2, 3, 11\}$.

3) The residues r_i are used to reconstruct the value Φ_Q by the CRT of (4) as:

$$\begin{aligned} \Phi_Q &= \mathrm{CRT}(r_1, r_2, \ldots, r_P) \cdot Q \\ &= \left\langle \sum_{i=1}^{p} r_i \cdot A_i \cdot \frac{M}{m_i} \right\rangle_M \cdot Q \end{aligned} \tag{11}$$

where A_i are the multiplicative inverses for the modulus m_i.

For the fractional part, not implemented in RNS, we introduce $\{\gamma_i\}$ defined as

$$\{\gamma_i\} = \gamma_i - \left\lfloor \frac{\gamma_i}{Q} \right\rfloor \cdot Q = \gamma_i - r_i \cdot Q \quad \forall i \in \{1, \ldots, P\} \tag{12}$$

with range $0 \leq \{\gamma_i\} < Q$.

Since the normalization in (9) and the quantum Q is the same for each track, the fractional parts are equal in each track/channel (ideal case):

$$\{\gamma_1\} = \{\gamma_2\} = \ldots = \{\gamma_P\}.$$

Consequently, the angle Φ_δ, fraction of Q, is computed as:

$$\Phi_\delta = \delta_\Phi \cdot Q \equiv \{\gamma_i\} \quad \forall i \in \{1, \ldots, P\} \tag{13}$$

As the last step, the reconstruction of the angle Φ is obtained by (7)

$$\Phi = \Phi_Q + \Phi_\delta \, .$$

TABLE 2. Example of angle reconstruction for the moduli set {2, 3, 11}.

EE parameters
$M = 66, Q = 360/66 = 5.45$

Inputs
$\varphi_1 = 210$, $\varphi_1 = 20$, and $\varphi_1 = 300$

Step 1: Expression (9)
$\gamma_1 = 6.3636$, $\gamma_2 = 0.9091$, and $\gamma_3 = 50.000$
Step 2: Using equation (10), we calculate the residues for each modulus m_i: $r_1 = 1$, $r_2 = 0$, and $r_3 = 9$, using Residue Number System (RNS) arithmetic.
Step 3: Using equation (11), we apply the Chinese Remainder Theorem (CRT) to compute the angle Φ_Q as $\Phi_Q = \mathrm{CRT}(1, 0, 9)Q = 49.0909$.
Fraction of Q: Using equation (13), we calculate the fractional part of the angle Φ_Q as $\Phi_\delta = \gamma_1 = \gamma_2 = \gamma_3 = 0.9091$.
Reconstructed angle: Finally, we obtain the reconstructed angle Φ by adding the angle Φ_Q and its fractional part Φ_δ: $\Phi = \Phi_Q + \Phi_\delta = 50°$.

FIGURE 6. The presence of noise in the angle measurement near the edge of an interval Q could create a jump of $\{\gamma_i\}$ to an adjacent interval.

In table 2, we present an example of angle reconstruction for the moduli set 2, 3, 11, where the input angles are $\varphi_1 = 210$, $\varphi_2 = 20$, and $\varphi_3 = 300$.

V. NOISE'S EFFECTS CHARACTERIZATION AND MITIGATION

The angle reconstruction in Section IV-A refers to the ideal condition where the plates are not affected by any deformations and the measurements of all φ_i are not affected by any kind of noise.

However, in a real environment, this is not true and the effects of the errors become more critical when measuring an angle close to the *edges* of the quantization interval. In this case, as shown in Fig. 6, mechanical deformations and noise, could introduce a "jump" of the measured value from a quantization interval to the adjacent one, resulting in a wrong value both for the integer part $r_i \cdot Q$ and for the fractional part $\{\gamma_i\}$ of the normalized angles of track i.

Considering a generic angle γ_i of track i, an unwanted jump from an interval Q_j to an adjacent interval $Q_{j\pm1}$, introduces a difference $\simeq 1$ of its fractional part with respect to the angles measured on the other tracks. As a consequence, expression (9) will return a wrong value, introducing an *error* in the computation of the *residue* r_i.

To mitigate these errors, the residues are computed in some cases using the *floor* function, as expressed in (10), while in other cases they are calculated by using the *round* function. In order to establish the proper rounding function, we use a *majority voting* approach on the fractional part of the measured $\{\gamma_i\}$. In the following, for each normalized angle γ_i, we assume a measurement error e_i limited to

$$e_i \leq N_{max} = \frac{Q}{4}.$$

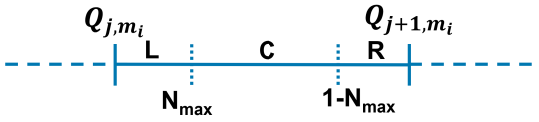

FIGURE 7. Sub-intervals L, C and R in interval $[Q_j,\ Q_{j+1}]$ (size $Q = 4N_{max}$).

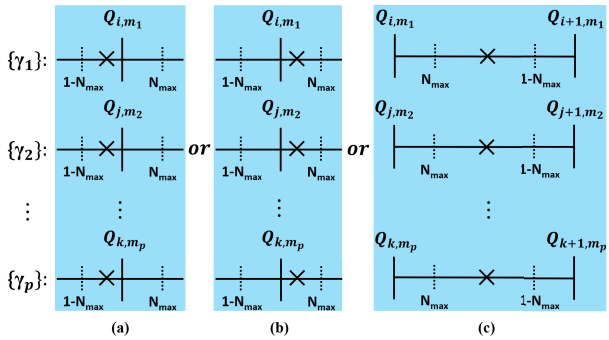

FIGURE 8. Case 1: all fractional parts of the three moduli are at the same time in the same sub-interval: (a) $\{\gamma_i\} > 1 - N_{max}$; (b) $\{\gamma_i\} < N_{max}$; (c) $N_{max} < \{\gamma_i\} < 1 - N_{max}$;.

For our system, N_{max} represents the maximum noise which guarantees an angular reconstruction with limited error (comparable or less than the initial errors e_i). By using N_{max}, each interval Q is divided into three sub-intervals:

1) *sub-interval s.L* $\{\gamma_i\} < N_{max}$
2) *sub-interval s.C* $N_{max} \leq \{\gamma_i\} \leq 1 - N_{max}$
3) *sub-interval s.R* $\{\gamma_i\} > 1 - N_{max}$

where L, C, and R stand for *Left, Center, Right*, respectively.

A graphical representation of these three sub-intervals is shown in Fig. 7.

In these settings, whether there is a measurement error $e_i < \pm N_{max}$ on a given track and there are no jumps to adjacent intervals the absolute angle reconstructed, after applying the CRT, can be affected by an error $\leq e_i$ due to the averaging process of the reconstruction of $\{\gamma_i\}$. In contrast, if the error is such that the measured angle jumps to the adjacent quantization interval, the output result could be totally wrong. If jumps occur, even for small errors, the corresponding residual r_i is incorrect and the angle reconstructed by the CRT is totally wrong, if no recovery technique is applied. To overcome these problems, we can introduce suitable recovery techniques, considering three different cases.

A. CASE 1

In the first case, depicted in Fig. 8, all $\{\gamma_i\}$, represented by symbol $\times$, are at the same time in the correct sub-interval of Q.

In Figure 8 there are no jumps to adjacent Q intervals, so the noise affects the measurement in a limited way. The residues r_i are computed as the integer part (*floor* function) of γ_i as shown in (10), while $\Phi_\delta = \{\Phi\}$ is computed as the average of all $\{\gamma_i\}$ as expressed in (14). Note that averaging has a low pass effect on the noise.

$$\{\Phi\} \equiv \theta_a = \frac{\sum_{i=1}^{P}\{\gamma_i\}}{P} \tag{14}$$

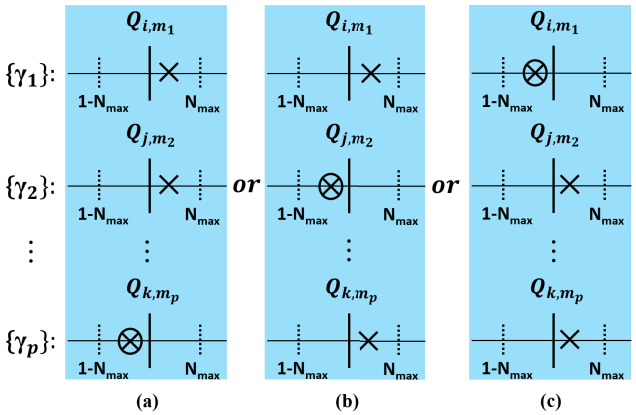

FIGURE 9. Case 2: one or more $\{\gamma_i\}$ jumps from the sub-interval *s.L* to the sub-interval *s.R* of the previous quantization interval.

The same computations hold, for error shifts from the sub-intervals *s.L* and *s.R* to *s.C*, or vice versa.

B. CASE 2

In the second case, depicted in Fig. 9, one or more jumps, represented by the symbol $\otimes$, to an adjacent Q interval occur. We consider in this case only jumps from the correct sub-interval *s.L* to the *s.R* of the previous Q interval. However, we assume that the majority of $\{\gamma_i\}$ are in the correct sub-interval *s.L*.

The capability of the system to detect and correct these jumps depends on the number of moduli P. The number of errors (jumps) that can be detected are $D_{max} = \lfloor \frac{P}{2} \rfloor$, while the number of possible corrections is $C_{max} = \lceil \frac{P}{2} - 1 \rceil$. For this reason, with two traces the system is able only to detect one error without correction ability, while with three traces the system is able to detect and correct one error.

Taking into account the maximum number and the maximum amplitude allowed for the errors, we can detect the jumps in Figure 9 by considering the values of $\{\gamma_i\}$ for the different tracks/moduli.

Jumps from *s.L* to *s.C* do not represent an issue since they end up in the same interval. However, if the majority of $\{\gamma_i\}$ lie in the sub-interval *s.L*, and some $\{\gamma_i\}$ lie in the sub-interval *s.C*, the latter are computed in the average only if $\{\gamma_i\} < 0.5\ Q$. In this case, the residues r_i are computed using the *round* function:

$$r_i = round\left(\frac{\gamma_i}{Q}\right) \qquad i = 1, 2, \ldots, P \tag{15}$$

For the angle fractional part, the $\{\Phi\}$ value is the average of the P_{NJ} $\{\gamma_i\}$ not affected by jumps of the quantization interval, corresponding to all $\{\gamma_i\} < 0.5\ Q$. Since the system is able to correct C_{max} errors due to jumps to a different quantization interval, the number of moduli not affected by interval jumps can be in the worst case $P_{NJ} = P - C_{max} = \lfloor \frac{P}{2} + 1 \rfloor$. As a consequence, with P moduli, the $\{\Phi\}$ value is set as the average θ_l of the P_{NJ} fractional angles $\{\gamma_i\}$ not affected by

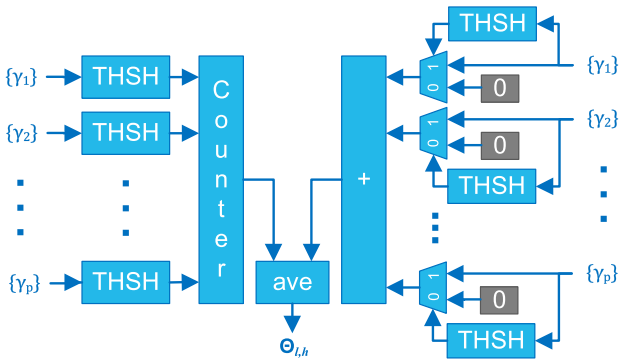

FIGURE 10. Block diagram to compute θ_l (θ_h) when the majority of $\{\gamma_i\}$ is below (above) the threshold.

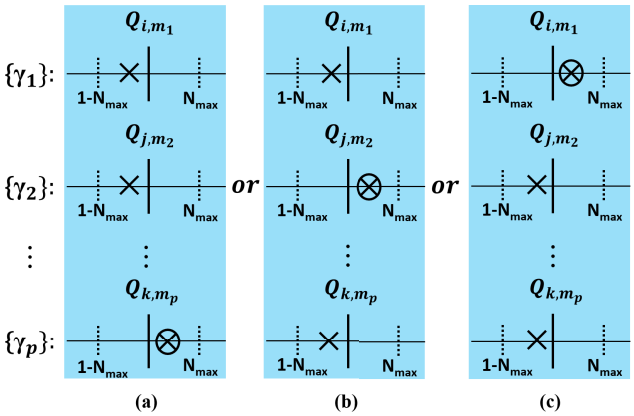

FIGURE 11. Case 3: one or more $\{\gamma_i\}$ jumps from the sub-interval *s.R* to the sub-interval *s.L* of the next quantization interval.

jump errors

$$\{\Phi\} \equiv \theta_l = \frac{\sum_{i=1}^{P_{NJ}} \{\gamma_i\}}{P_{NJ}} \tag{16}$$

A block diagram to compute by averaging (16) $\{\Phi\} = \theta_l$ is shown in Fig. 10. Block THSH (THreSHold) checks if the input is below, or above, a given threshold. It is implemented by a 2's complement comparator with 1-bit output: the sign of the comparison. The right-hand side of Figure 10 conditionally adds all γ_i below the set threshold (THSH=0.5), the numerator of (16), while the left-hand side, counts the number of γ_i satisfying the threshold condition, the denominator of (16). The result θ_l is therefore the average of all $\gamma_i < 0.5$ for case 2. The block *counter* is an adder of bits with the same weight, while the *ave* block computes the average based on P_{NJ}.

C. CASE 3

In the third case, depicted in Fig. 11, one or more $\{\gamma_i\}$ jumps from the sub-interval *s.R* to the sub-interval *s.L* of the next quantization interval occur.

In Figure 11 the majority of $\{\gamma_i\}$ are in the sub-interval *s.R* (or in *s.C* with $\{\gamma_i\} > 0.5\ Q$).

TABLE 3. Computation of residues r_i and $\{\Phi\}$ values.

	Case	Residues r_i	$\{\Phi\}$
1	All $\{\gamma_i\}$ are in the same sub-interval	*(floor)* $r_i = \lfloor \gamma_i \rfloor$	$\{\Phi\} = \theta_a$
2	All $\{\gamma_i\}$ are NOT in the same sub-interval - if majority $\{\gamma_i\} < 0.5Q$	*(round)* $r_i = \lfloor \gamma_i \rceil$	$\{\Phi\} = \theta_l$
3	- if majority $\{\gamma_i\} > 0.5Q$	$r_i = \lfloor \gamma_i \rceil - 1$	$\{\Phi\} = \theta_h$

In this case, since the $\{\gamma_i\} > 0.5Q$, the residues are computed by rounding (to Q_{j+1}) followed by a decrement

$$r_i = round\left(\frac{\gamma_i}{Q}\right) - 1 \qquad i = 1, 2, \ldots, P \tag{17}$$

The fractional value $\theta_h = \{\Phi\}$ is obtained by averaging the fractional angles $\{\gamma_i\} > 0.5Q$, as in (16). The block diagram in Figure 10 is used to compute θ_h by swapping the comparators' inputs in blocks THSH.

D. HARDWARE IMPLEMENTATION

The block diagram of the complete system for error detecting and correction is shown in Fig. 12.

The measured angles φ_i are firstly normalized by the block *Angle Normalization*, implementing (9), and the obtained values are split into two separated paths: one for the computation of the integer part, and one for the computation of fractional part (*fraction { } block)*.

In the integer part (left-hand side of Figure 12), both the *floor* and *round* functions are computed, and the rounded value is eventually updated (control signal *SubR*), and the residues r_i are produced by selecting (control signal *Round*) the values according to the three cases listed in Section V-A–V-C and summarized in Table 3. The RNS residues r_i are converted by the CRT block to obtain the integer part of Φ.

In the fractional part (right hand side of Figure 12), from the P inputs $\{\gamma_i\}$ the fractional values of the angles $\{\Phi\}$ is computed by selecting the correct value among the results generated by the block Θ_a (implementing (14)) and the block $\Theta_{h/l}$ (implementing (16)) and depicted by the block diagram of Fig. 10.

The architecture of Figure 12 is completed by the adder and scaling blocks (at bottom left) to reconstruct the angle Φ. Expression (7) is rewritten to match the symbols in the figure as

$$\Phi = (\ \lfloor \Phi \rfloor\ +\ \{\Phi\}\ ) \cdot Q$$

The block *Enable Round/SubR* at the far right of Figure 12 generates the control signals necessary to select the actual case among the ones in Table 3. The inputs $\{\gamma_i\}$ are compared with a number of thresholds, corresponding to the different sub-interval segments, to activate the correct rounding function according to Table 3. If some $\{\gamma_i\}$ are in both the *s.L* and *s.C* sub-intervals, rounding is required and the *Round* signal is activated.

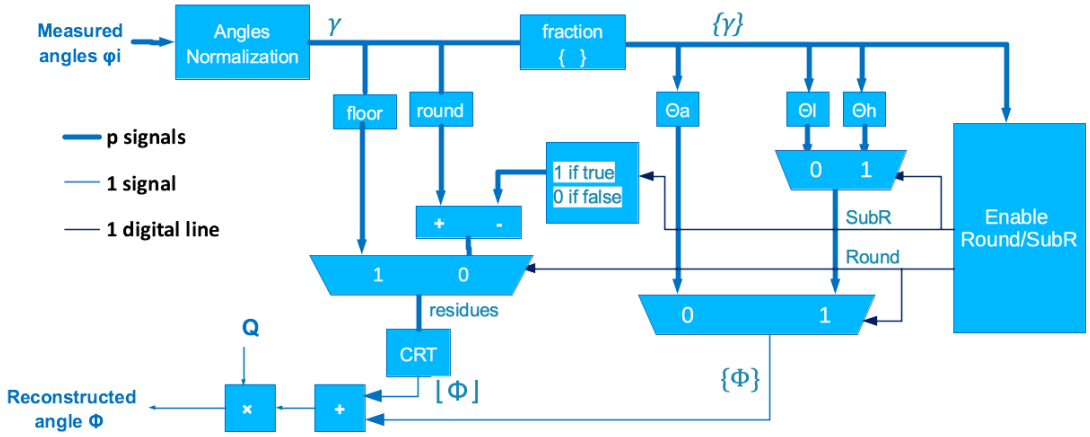

FIGURE 12. The main blocks used to estimate the initial position taking into account of measurement errors within $\pm N_{max}$. The inputs of the system are the measured angles φ_i of each trace and the output is the reconstructed absolute angle Φ.

In addition, the *Enable Round/SubR* unit evaluates the positions of the majority of $\{\gamma_i\}$, and if they are in $s.C$ the signal *SubR* is activated to perform $r_i = \lfloor \gamma_i \rceil - 1$.

An example of angle reconstruction in presence of noise, and error-detection and correction implemented, is shown in Fig. 13. The noise, in this context, is used to emulate some unwanted real phenomena, such as thermal noise, mechanical imperfection, vibrations, electromagnetic noise, etc. In real applications, all these effects may produce the wrong read value of the angle on one or more traces. To emulate these unwanted phenomena, the authors first created a data set by sampling the 360° angle with 0.01° steps (36000 values) and added to each sample a random value between $-N_max$ and $+N_max$. To generate these values to be added to the read angle, the authors generated 36000 random values following a Gaussian distribution because most of them should be 0-centered as it happens in real cases. However, even if we use other types of noise the result is exactly the same because the samples that are used for both angle estimation and error detection are uncorrelated. The system parameters are: $P = 3$, $m_i \in \{2, 3, 11\}$, M=66 and Q=5.4545°. The upper graph (Fig. 13.a) represents the input of the system, i.e., the measured absolute angle which varies from 0° to 360° with an angular step of $\Delta\Phi = 0.001°$. By applying additive white gaussian noise, or AWGN, several measurement errors appear in Fig. 13.b. Since the noise introduces angular errors smaller than $N_{max} = Q/4 = 1.36°$, the system is able to correct them and the reconstructed angle is shown in the third graph (Fig. 13.c). The graph at the bottom (Fig. 13.d) shows the error distribution for the reconstructed angle with AWGN (i.e. the difference between the input angle and the reconstructed one). The average and maximum errors are:

$$e_{average} = 6.7 \cdot 10^{-3} \text{ and } |e_{max}| = 1.4 \cdot 10^{-2}.$$

VI. THE CHOICE OF MODULI AND THE NUMBER OF REVOLUTION PERIODS IN AN EE

Since the quantity N_{max} depends on interval Q, the system is more tolerant if this interval is larger. This corresponds

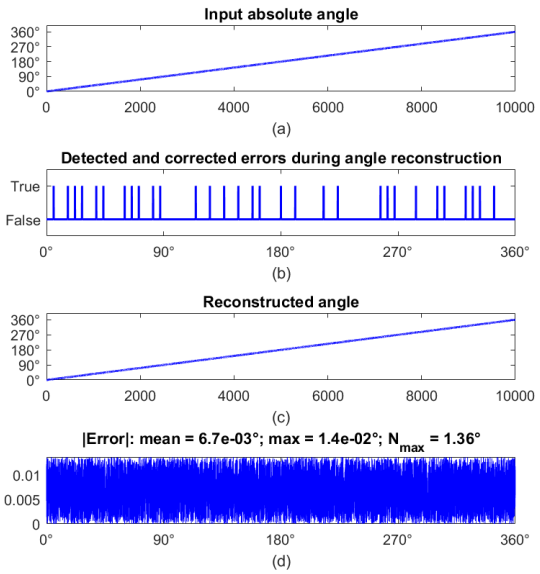

FIGURE 13. Applying noise to the input angle (a) , the system detects and corrects the errors (b) and finally reconstructs the angle (c). The resulting noise in the output is shown in (d).

to choosing traces with the least possible number of revolutions per trace *rpt* (i.e., small values of M). However, the final choice must also take into account the resolution Q of the measurement. The algorithm shown in this work is used only for the computation of the initial position in an EE. Afterward, the system calculates the following positions by integrating the newly measured angles of a single trace. In other words, the variation of the measured angle $\Delta\varphi_i$ in the reference, trace is added to the initial (previous) value. The reference trace used for these successive computations is the one with the smaller modulus m_i representing the trace with the higher number of *rpt*. This choice is justified by the relationship, derived from (9), between the absolute angle Φ and the *local* angles φ_i of each modulus:

$$\varphi_i = \left\langle \frac{\Phi \cdot M}{m_i} \right\rangle_{360°} = \langle \Phi \cdot K_i \rangle_{360°} \tag{18}$$

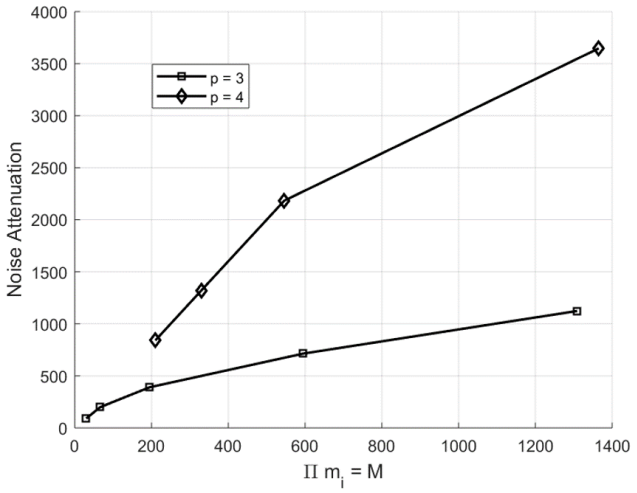

FIGURE 14. Noise attenuation with varying *P* and *M*.

In (18), a small variation of Φ is amplified K_i times in the angle φ_i. That is,

$$\Delta\varphi_i = \Delta\Phi \cdot K_i \tag{19}$$

From (19), we define in (20) the quantity $G_{s,i} = K_i$ representing the sensitivity gain of modular angle φ_i:

$$G_{s,i} = \frac{\Delta\varphi_i}{\Delta\Phi} = \frac{M}{m_i} = K_i \tag{20}$$

Since the sensitivity of a modular angle φ_i with respect to the absolute angle Φ is directly proportional to $G_{s,i}$ and then to K_i, we have to find a trade-off between N_{max} and $G_{s,i}$ given by

$$G_{s,i} = \frac{360^\circ}{4{\cdot}N_{max} \cdot m_i} \tag{21}$$

A reasonable choice could be to use $P-1$ moduli with as small as possible values, while the *P-th* modulus should be chosen to match the desired sensitivity. If we consider $P = 3$, the best configuration for noise tolerance is the one having moduli $m_i \in \{2, 3, 5\}$. In this case, the maximum sensitivity gain useful for the computation of successive positions is given by using the modulus $m_1 = 2$ with $G_{s,1} = 15$. However, if we want to improve the sensitivity, we can increase the value of m_3 from 5 to 11, doubling the sensitivity gain from 15 to 33.

Commercial EEs have traces revolving up to 128 *rpt* (traces with more *rpt* are physically very difficult to realize), and a number of *rpt*s in this range can be represented by a moduli-set such as $m_i \in \{3, 8, 15\}$.

A. NOISE ATTENUATION WITH VARYING P AND M

Another important aspect to consider is the relationship between the tolerance to the noise and the number of moduli *P*. Fig. 14 plots the system noise attenuation using three and four moduli ($P = 3$ and $P = 4$) for different values of *M*. The experiments are performed applying a uniform noise distribution between $\pm N_{max}$, to the smallest modulus m_1, for each of the (P, M) pairings. The plots in Figure 14 show that a larger *P* improves the system's capability to attenuate noise at a comparable dynamic range *M*.

VII. CONCLUSION

In this work, we present a system to estimate the initial position of a type of electrical encoder by using the RNS representation and the CRT algorithm for the reconstruction of the measured angle. With respect to previous work, we generalize the reconstruction algorithm to handle systems with more than two tracks and add robustness to the reconstruction by detection and correction of errors due to noise, when less than N_{max}. The proposed approach is very flexible and reconfigurable by choosing the set of moduli satisfying the design constraints. Since the moduli set influences the noise robustness and the sensitivity of the measurement, the best choice can be made by considering their trade-off.

An improvement, for future work, is to have a redundant set of moduli to be able to correct measurement errors also in presence of noise greater than N_{max}.

REFERENCES

[1] N. S. Szabo and R. I. Tanaka, *Residue Arithmetic and Its Applications to Computer Technology*, New York, NY, USA: McGraw-Hill, 1967.
[2] P. V. A. Mohan, *Residue Number Systems: Algorithms and Architectures*. Cham, Switzerland: Springer, 2002.
[3] G. C. Cardarilli, A. Nannarelli, and M. Re, "RNS applications in digital signal processing," in *Embedded Systems Design with Special Arithmetic and Number Systems*. Cham, Switzerland: Springer, 2017, pp. 181–215.
[4] G. C. Cardarilli, L. D. Nunzio, R. Fazzolari, A. Nannarelli, M. Petricca, and M. Re, "Design space exploration based methodology for residue number system digital filters implementation," *IEEE Trans. Emerg. Topics Comput.*, vol. 10, no. 1, pp. 186–198, Jan. 2022, doi: 10.1109/TETC.2020.2997067.
[5] H. Nakahara and T. Sasao, "A high-speed low-power deep neural network on an FPGA based on the nested RNS: Applied to an object detector," in *Proc. IEEE Int. Symp. Circuits Syst. (ISCAS)*, May 2018, pp. 1–5.
[6] K. Givaki, R. Hojabr, M. H. Gholamrezaei, A. Khonsari, S. Gorgin, D. Rahmati, and M. H. Najafi, "High-performance deterministic stochastic computing using residue number system," *IEEE Design Test*, vol. 38, no. 6, pp. 60–68, Dec. 2021, doi: 10.1109/MDAT.2021.3051848.
[7] P. Lyakhov, M. Valueva, G. Valuev, and N. Nagornov, "High-performance digital filtering on truncated multiply-accumulate units in the residue number system," *IEEE Access*, vol. 8, pp. 209181–209190, 2020.
[8] C.-H. Chang, A. S. Molahosseini, A. A. E. Zarandi, and T. F. Tay, "Residue number systems: A new paradigm to datapath optimization for low-power and high-performance digital signal processing applications," *IEEE Circuits Syst. Mag.*, vol. 15, no. 4, pp. 26–44, 4th Quart., 2015.
[9] A.S. Molahosseini, A. A. E. Zarandi, P. Martins, and L. Sousa, "A multifunctional unit for designing efficient RNS-based datapaths," *IEEE Access*, vol. 5, pp. 25972–25986, 2017.
[10] P. Boyvalenkov, N. I. Chervyakov, P. Lyakhov, N. Semyonova, A. Nazarov, M. Valueva, G. Boyvalenkov, D. Bogaevskiy, and D. Kaplun, "Classification of moduli sets for residue number system with special diagonal functions," *IEEE Access*, vol. 8, pp. 156104–156116, 2020.
[11] P. Martins and L. Sousa, "The role of non-positional arithmetic on efficient emerging cryptographic algorithms," *IEEE Access*, vol. 8, pp. 59533–59549, 2020.
[12] G. C. Cardarilli, L. Di Nunzio, R. Fazzolari, L. Gerardi, M. Re, G. Campolo, and D. Cascone, "A new electric encoder position estimator based on the Chinese remainder theorem for the CMG performance improvements," in *Proc. IEEE Int. Symp. Circuits Syst. (ISCAS)*, May 2017, pp. 1–4.
[13] *Netzer Precision Position Sensors*. Accessed: Jul. 2023. [Online]. Available: https://netzerprecision.com/

[14] *Application Note 02 Electrically Interfacing DS Electric Encoders*, Netzer Precision Motion Sensors Ltd, Misgav Industrial Park, Jerusalem, Israel, 2009.
[15] *Application Note 03 Absolute Angle Computation*, Netzer Precision Motion Sensors Ltd, Misgav Industrial Park, Jerusalem, Israel, 2009.
[16] N. Yishay, "Capacitive displacement encored," U.S. Patent WO 02 31 432 A2, Apr. 18, 2002.
[17] M. A. Soderstrand and K. Al-Marayati, "VLSI implementation of very-high-order FIR filters," in *Proc. Int. Symp. Circuits Syst.*, Apr. 1995, pp. 1436–1439.

GIAN CARLO CARDARILLI (Member, IEEE) was born in Rome, Italy. He received the "Laurea" degree (summa cum laude) from the University of Rome "La Sapienza," Italy, in 1981. He has been with the University of Rome "Tor Vergata," Italy, since 1984, where he is currently a Full Professor in digital electronics and electronics for communication systems with the Department of Electronic Engineering. From 1992 to 1994, he was with the University of L'Aquila, Italy. From 1987 to 1988, he was with the Circuits and Systems Team, EPFL, Lausanne, Switzerland. His research interests include VLSI architectures for signal processing and IC design. In this field, he has published more than 160 papers in international journals and conferences. He has also regular cooperation with companies, such as Alcatel Alenia Space, Italy; STM, Agrate Brianza, Italy; Micron, Italy; and Selex S.I., Italy. His scientific interest concerns the design of special architectures for signal processing. He works in the field of computer arithmetic and its application to the design of fast signal digital processor.

LUCA DI NUNZIO was born in Pescara, Italy. He received the master's degree (summa cum laude) in electronics engineering and the Ph.D. degree in systems and technologies for space applications from the University of Rome "Tor Vergata," Italy, in 2006 and 2010, respectively. He has a working history with several companies in the fields of electronics and communications. He is currently an Adjunct Professor with the Digital Electronics Laboratory, University of Rome "Tor Vergata," and an Adjunct Professor in digital electronics with University "Guglielmo Marconi," Italy. His research interests include reconfigurable computing, communication circuits, digital signal processing, and machine learning.

ROCCO FAZZOLARI received the M.S. degree in electronic engineering and the Ph.D. degree in space systems and technologies from the University of Rome "Tor Vergata," Italy, in May 2009 and June 2013, respectively. He is currently an Assistant Professor in digital electronics with the Department of Electronic Engineering, University of Rome "Tor Vergata." He works on the hardware implementation of high-speed systems for digital signals processing, machine learning, and low power digital systems.

DANIELE GIARDINO received the B.S. and M.S. degrees in electronic engineering from the University of Rome "Tor Vergata," Italy, in 2015 and 2017, respectively, where he is currently pursuing the Ph.D. degree in electronic engineering. He is also a member of the Research Group DSPVLSI. He works on digital development for wideband signals architectures, telecommunications, digital signal processing, and machine learning. In specific, he is focused on the digital implementation of MIMO systems for wideband signals.

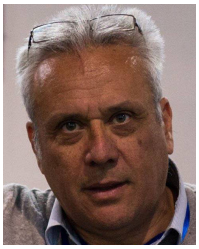

MARCO RE (Member, IEEE) received the Ph.D. degree in microelectronics from the University of Rome "Tor Vergata," Italy. He is currently an Associate Professor with the Department of Electronic Engineering, University of Rome "Tor Vergata," where he teaches digital electronics and hardware architectures for DSP. He was awarded with two NATO fellowships with the University of California at Berkeley, USA, as a Visiting Scientist with the Cadence Berkeley Laboratories. He has been awarded with the Otto Moensted Fellowship as a Visiting Professor with the Technical University of Denmark. He collaborates in many research projects with different companies in the field of DSP architectures and algorithms. His research interests include low power DSP algorithms architectures, hardware-software codesign, fuzzy logic and neural hardware architectures, low power digital implementations based on non-traditional number systems, computer arithmetic, and CAD tools for DSP. He is the author of about 200 papers in international journals and international conferences. He is a member of Audio Engineering Society (AES). He is also the Director of the Master in Audio Engineering with the University of Rome "Tor Vergata."

ALBERTO NANNARELLI (Senior Member, IEEE) received the Graduate degree in electrical engineering from the University of Rome "La Sapienza," Italy, in 1988, and the M.S. and Ph.D. degrees in electrical and computer engineering from the University of California at Irvine, USA, in 1995 and 1999, respectively. He is currently an Associate Professor with the Technical University of Denmark, Lyngby, Denmark. He worked for SGS-Thomson Microelectronics and for Ericsson Telecom as a Design Engineer and Rockwell Semiconductor Systems as a Summer Intern. From 1999 to 2003, he was with the Department of Electronic Engineering, University of Rome "Tor Vergata," Italy, as a Postdoctoral Researcher. His research interests include computer arithmetic, computer architecture, and VLSI design. He is a Senior Member of the IEEE Computer Society.

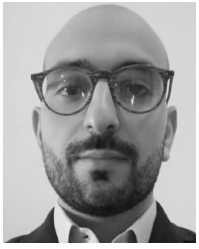

SERGIO SPANÒ received the B.S. degree in electronic engineering and the M.S. degree (summa cum laude) in electronic engineering from the University of "Tor Vergata," Rome, Italy, in 2015 and 2018, respectively, where he is currently pursuing the Ph.D. degree in electronic engineering. He is also a member of the DSPVLSI Research Group, University of "Tor Vergata." His research interests include digital signal processing, machine learning, telecommunications, and ASIC/FPGA hardware design. He had industrial experiences in the space and telecommunications field. His current research interest includes machine learning hardware implementations for embedded and low-power systems.

Open Access funding provided by 'Università degli Studi di Roma "Tor Vergata"' within the CRUI CARE Agreement